Key Points:

- Stratospheric moistening after 2000 is clearly detectable in ERA5-driven simulations, satellite and in situ observations
- Hemispheric asymmetry is found with strong positive trends in the Northern Hemisphere and weak negative trends over the South Pole
- Moistening of the lower tropical stratosphere is only partially caused by El Nino-Southern Oscillation and volcanic eruptions

Stratospheric Moistening After 2000

Paul Konopka[1] [ID]**, Mengchu Tao[2], Felix Ploeger[1]** [ID]**, Dale F. Hurst[3,4]** [ID]**, Michelle L. Santee[5]** [ID]**, Jonathon S. Wright[6]** [ID]**, and Martin Riese[1]** [ID]

[1]Forschungszentrum Jülich, Jülich, Germany, [2]Carbon Neutrality Research Center, Institute of Atmospheric Physics, Beijing, China, [3]Cooperative Institute for Research in Environmental Sciences, University of Colorado, Boulder, CO, USA, [4]Global Monitoring Laboratory, NOAA Earth System Research Laboratories, Boulder, CO, USA, [5]Jet Propulsion Laboratory, California Institute of Technology, Pasadena, CA, USA, [6]Department of Earth System Science, Tsinghua University, Beijing, China

Abstract The significant climate feedback of stratospheric water vapor (SWV) necessitates quantitative estimates of SWV budget changes. Model simulations driven by the newest European Centre for Medium-Range Weather Forecast reanalysis ERA5, satellite observations from the Stratospheric Water and OzOne Satellite Homogenized data set, Microwave Limb Sounder, and in situ frost point hygrometer observations from Boulder all show substantial and persistent stratospheric moistening after a sharp drop in water vapor at the turn of the millennium. This moistening occurred mainly during 2000–2006 and SWV abundances then remained high over the last decade. We find strong positive trends in the Northern Hemisphere and weak negative trends over the South Pole, mainly during austral winter. Moistening of the tropical stratosphere after 2000 occurred during late boreal winter/spring, reached values of ~0.2 ppm/decade, was well correlated with a warming of the cold point tropopause by ~0.4 K/decade and can only be partially attributed to El Nino-Southern Oscillation and volcanic eruptions.

Plain Language Summary Water vapor is an effective greenhouse gas. Human-induced climate change has led to warmer air in the troposphere, which consequently can hold more moisture, thus enhancing the greenhouse effect. The long-term change in stratospheric water vapor (SWV) is less clear and currently under debate. Using satellite observations, balloon soundings and model simulations, we find an increase of SWV after 2000. This moistening occurred mainly during 2000–2006 and the stratospheric moisture content then remained high over the last decade. The increase of SWV is stronger in the Northern than in the Southern Hemisphere. Over the South Pole, a weak decrease was found. Moistening of the tropical stratosphere occurred mainly during late winter and spring, and was in line with warming of the tropical tropopause, the coldest region that separates the troposphere and stratosphere. Natural causes such as volcanic eruptions cannot completely explain this stratospheric moistening.

1. Introduction

Stratospheric water vapor (SWV) plays a significant role in the positive feedback of global climate warming, with a radiative forcing around 0.25 W/m² for each 1 ppm increase (Forster & Shine, 1999; Solomon et al., 2010) and with feedback values between 0.1 and 0.3 W/m²/K (Banerjee et al., 2019; Li & Newman, 2020). Long-term, routine balloon-borne measurements are rare (Müller et al., 2016), with the longest available record being that from the balloon-borne NOAA frost point hygrometer over Boulder (Boulder/FPH), Colorado, USA starting in 1980 (Hurst et al., 2011). Observations by multiple satellite instruments with better spatial coverage but relatively short lifetimes have to be bias-corrected before trend analysis can be performed (Hegglin et al., 2014). Observation-based estimates of the SWV trends in the Northern Hemisphere midlatitude lower stratosphere vary between positive values of 0.05 ppm per year before 2000 (Oltmans et al., 2000; Rosenlof et al., 2001; Solomon et al., 2010) and a decrease after 2000 (Hegglin et al., 2014). Thus, robust estimation of a global SWV trend (i.e., as a function of latitude and altitude) over the last 40 years remains a challenge even though climate models, almost unanimously, project future stratospheric moistening (Keeble et al., 2021). The largest contribution to SWV feedback (66%–75%) is expected to be caused by increasing SWV in the lowermost stratosphere due to climate change (Banerjee et al., 2019; Dessler et al., 2013; Li & Newman, 2020).

Lagrangian (i.e., trajectory-based) models driven by meteorological reanalyses reproduce observed SWV mixing ratios well (Smith et al., 2021; Tao et al., 2019, and references therein). This is mainly because dehydration at the

tropical cold point tropopause primarily controls the entry value of water vapor to the stratosphere (Brewer, 1949; Randel & Park, 2019) and such temperatures are provided with high quality by modern reanalyses (Fujiwara et al., 2017; Tegtmeier et al., 2020). Furthermore, trajectory-based models are able to sample these very low temperatures without numerical diffusion causing spurious moistening of the stratosphere (Fueglistaler & Haynes, 2005; Stenke et al., 2009). In this study, we apply the Chemical Lagrangian Model of the Stratosphere (CLaMS) driven by the newest generation reanalysis product ERA5 (Hersbach et al., 2020) of the European Centre for Medium-Range Weather Forecasts (ECMWF) to reconstruct SWV over the last 42 years. Comparison of our simulations with Boulder/FPH observations (Hurst et al., 2011) and with the recent Aura Microwave Limb Sounder (MLS) retrieval of SWV (Livesey et al., 2021) provides new insights into global SWV trends, especially in the stratospheric overworld.

2. Data and Methods

CLaMS is driven by prescribed meteorology with transport and chemistry calculated along 3D forward trajectories and an additional parameterized representation of atmospheric small-scale mixing processes (Konopka et al., 2004; McKenna et al., 2002). Model set-up is described in Pommrich et al. (2014); see Tao et al. (2019) for details of the SWV-related chemistry and microphysics. The lower boundary for water vapor is taken from the specific humidity (SH) below about 500 hPa provided by the reanalysis. Because of the dominant role of freeze drying at the Lagrangian cold point temperature (CPT), the exact tropospheric water vapor values have a minor influence on stratospheric entry values. The ERA5-driven model runs and their postprocessing are exactly the same as in Ploeger et al. (2021) (i.e., including the update named ERA5.1). In addition to ERA5, three other reanalyses are used: ERA-Interim (Dee et al., 2011), JRA-55 (Kobayashi et al., 2015), and MERRA-2 (Gelaro et al., 2017) using the same CLaMS simulations as those described in Tao et al. (2019). In addition, SH provided by ERA5 (SH/ERA5) is employed for trend analysis below the tropopause. Using independent satellite observations, Wang et al. (2020) have shown a significantly improved quality of this product compared with other reanalyses (Davis et al., 2017). Thus, zonally averaged monthly means of CLaMS SWV and SH/ERA5 are used in this study with pressure p and potential temperature θ denoting the vertical coordinate. CLaMS SWV and SH/ERA5 cover the period 1979–2020 while the other reanalysis-driven CLaMS runs are from 1980 to 2017. The Stratospheric Water and OzOne Satellite Homogenized (SWOOSH) data set version 2.5 (Davis et al., 2016) until 2005 and the latest version 5 MLS data (Livesey et al., 2020) from 2005 to 2020 are combined (SWOOSH/MLS) and, together with Boulder/FPH record from 1980 through 2020, are applied for model validation and trend analysis. Compared to MLS version 4 (used in the SWOOSH version 2.5), version 5 has reduced drifts relative to Boulder/FPH (Hurst et al., 2016; Livesey et al., 2021).

To analyze trends, multi-linear regression (MLR) is applied with regressors quantifying the Quasi-Biennial-Oscillation (QBO), the El Nino-Southern Oscillation (ENSO), and volcanic eruptions (El Chichon, Pinatubo and a few minor extratropical volcanoes after 2000) in terms of Aerosol Optical Depth (AOD; see lower panel of Figure 1). AOD is derived from the mean tropical (20°S–20°N) aerosol extinction coefficient ($\lambda = 525$ nm) averaged between the tropopause and 40 km altitude as provided by GLoSSAC v2.0 data (Kovilakam et al., 2020; Thomason, 2020) and is about an order of magnitude smaller during the period after 2000 than before. The Multivariate ENSO Index (MEI; Wolter & Timlin, 2011) is applied for ENSO. Zonal wind records at 50 and 30 hPa over Singapore provided by Freie Universität Berlin are employed for the QBO regression. Lagged regressors are used for ENSO and AOD to maximize correlations with the analyzed time series. Because two orthogonal QBO signals are used, it is not necessary to lag the QBO signal. The lag times are approximated as $f(\phi, \theta)$, with ϕ denoting latitude and θ potential temperature, and are easier to determine in the tropical pipe than at high latitudes where the maxima of the lagged correlations are weak. Application of the lagged MLR reduces the standard deviation of the original time series by 35% in the tropics and less than 10% at high latitudes (not shown). Weighted linear regression after removing statistical outliers is applied for the Boulder/FPH record (Hurst et al., 2014), and simple (i.e., ordinary least squares) linear trends with and without the MLR adjustment are calculated for all other data sets. Trends with p-values smaller than 0.05 are considered statistically significant; 2σ errors (95% confidence) quantify their uncertainties.
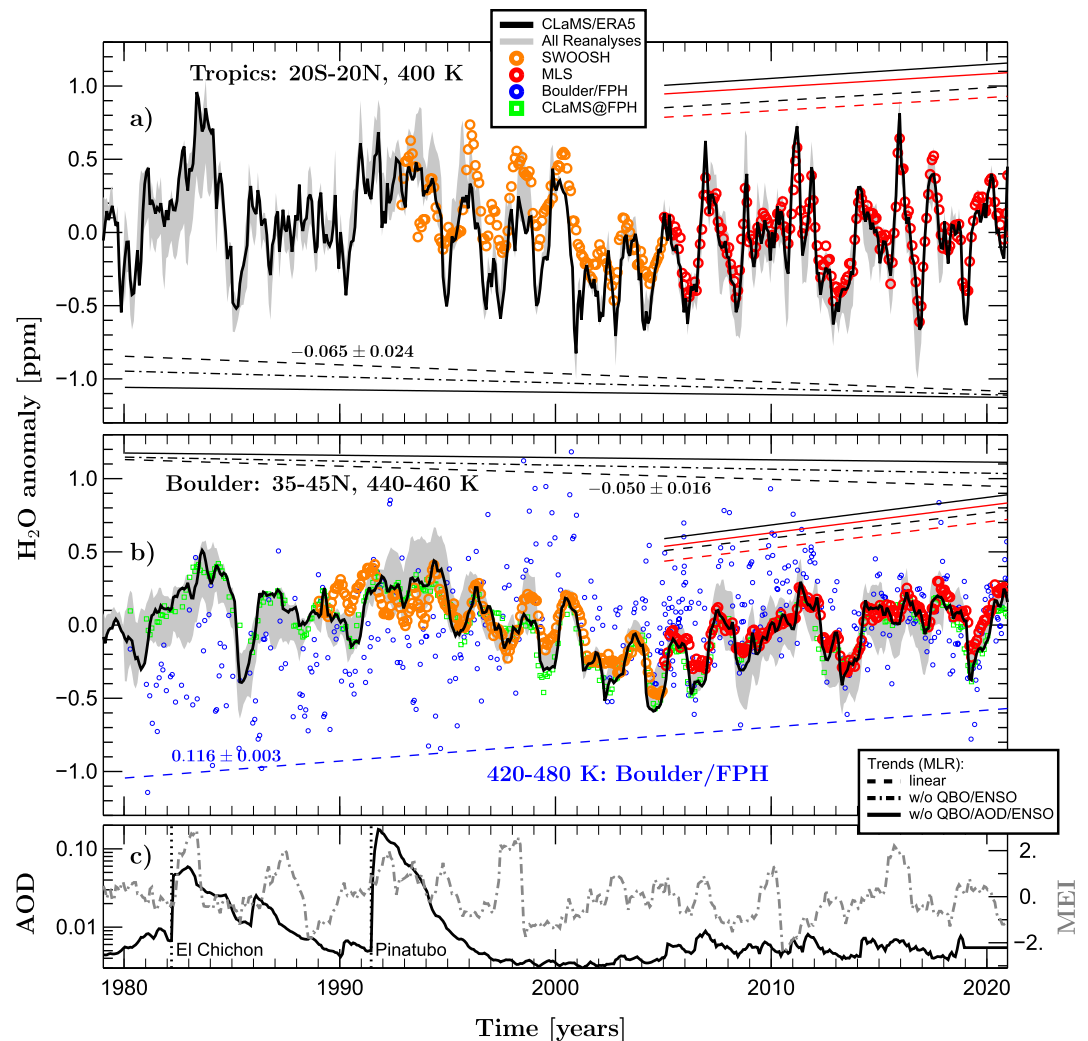
Figure 1. Deseasonalized and boxcar smoothed (width = 5 months) monthly mean stratospheric water vapor anomaly derived from Chemical Lagrangian Model of the Stratosphere (CLaMS)/ERA5 (black) and the spread among all reanalysis-based results (gray, for details, see supplement) for two regions in the lower stratosphere: Tropics (a) and Boulder (b). The Stratospheric Water and OzOne Satellite Homogenized, Microwave Limb Sounder and non-deseasonalized Boulder/FPH anomalies are overplotted with orange, red, and blue circles, respectively (CLaMS/ERA5 interpolated to Boulder/FPH measurement locations with green squares). Slopes of the lines quantify trends for the full and MLS periods (black—CLaMS/ERA5, red—MLS). Linear trends (in ppm/decade $\pm 2\sigma$) before and after multi-linear regression (MLR) adjustment to remove Quasi-Biennial-Oscillation/El Nino-Southern Oscillation/Aerosol Optical Depth signals are shown as dashed, dot-dashed, and solid lines (see legend). Only the linear trend is depicted for Boulder/FPH anomalies because the full MLR adjustment reduces their standard deviation by less than 6%. All linear trend values are listed in Table 1. (c) The Aerosol Optical Depth (AOD) derived from GLoSSAC v2.0 (a constant mean value calculated over 2013–2018 is used for the years 2019 and 2020) and the Multivariate El Nino-Southern Oscillation Index (MEI) are shown.

3. Results

To illustrate variations in stratospheric entry values of water vapor, we show in Figure 1a deseasonalized monthly mean SWV anomalies averaged between 20°S and 20°N at $\theta = 400$ K (Tropics). CLaMS/ERA5 and the spread among all reanalysis-based results are shown, along with SWOOSH and MLS data. All time series are boxcar smoothed (width = 5 months) to remove subseasonal variability. The lines visualize selected trends calculated for the 1980–2020 period and for the MLS period (2005–2020). For a further validation against Boulder/FPH data, the CLaMS, SWOOSH, and MLS anomalies are averaged over a zonal band containing Boulder (35°N–45° N, $440 \leq \theta \leq 460$) as shown in Figure 1b.
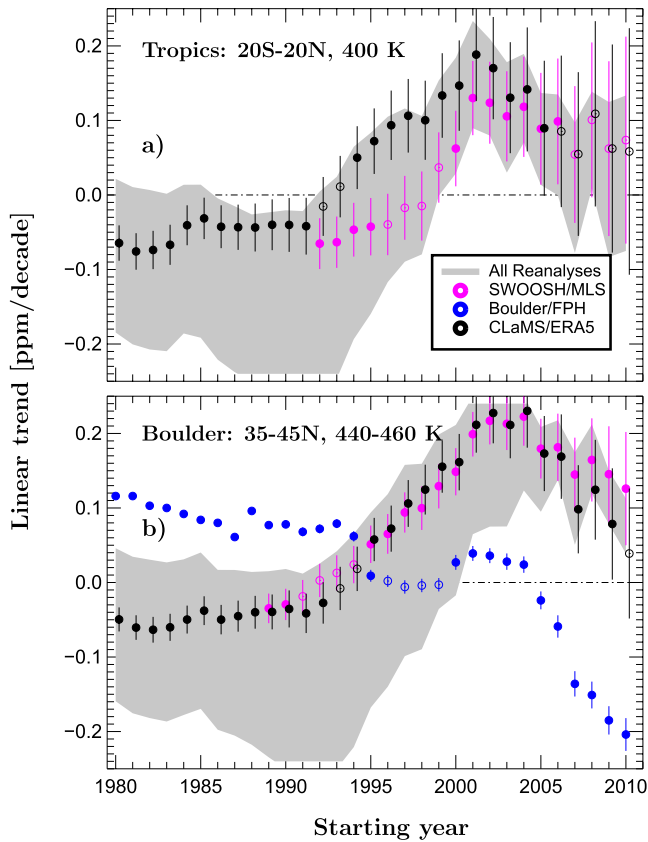
Figure 2. Sensitivity of the linear trends (through 2020) in (a) the Tropics and (b) the Boulder region to the choice of trend start year for different data sets listed in the legend. Only filled circles are statistically significant.

Boulder/FPH data are averaged over the θ-range 420–480 K to produce more meaningful statistics of SWV and to improve comparability with MLS water vapor observations, which have a vertical resolution of 2–3 km. Monthly means for the Boulder/FPH are predominantly based on single balloon soundings and, consequently, have quite large standard errors. Thus, removing a seasonal cycle from the Boulder/FPH time series adds more uncertainty; instead, we subtract 4.05 ppm (average and median of this record). Figure 1b shows the non-deseasonalized Boulder/FPH anomalies, with outliers removed following Hurst et al. (2014), and the corresponding 41-year weighted linear regression trend.

Trend analyses based on reanalysis products are inherently risky, as discontinuities may appear at any point when the density or quality of assimilated data changed (Fujiwara et al., 2017; Wright et al., 2022). Step-like improvements in CPT quality in many reanalyses have also been diagnosed around the TOVS-to-ATOVS transition in 1998–1999 and when COSMIC Global Navigation Satellite System-Radio Occultation data began to be assimilated in 2006 (Fueglistaler et al., 2013; Tegtmeier et al., 2020). As a general rule, the quality of the reanalyses decreases moving backward in time. We stress that the reanalysis-based trends should be interpreted with this caveat in mind, especially for the period before 2000, although good agreement with the SWOOSH data (Figure 1) strongly supports the reliability of the CLaMS/ERA5 variations in particular back to the early 1990s.

Linear trends in the tropical lower stratosphere, if calculated over the 1980–2020 period, are either negative or close to zero (and statistically insignificant) for all reanalysis-based simulations, with -0.065 ± 0.024 ppm/decade for CLaMS/ERA5 (see also Figure 2). After removing the moistening contributions of major volcanic eruptions (El Chichon—1982, Pinatubo—1991) and a few strong El Ninos in the 1980s and 1990s, the trend for CLaMS/ERA5 is statistically indistinguishable from zero (Figure 1a). This behavior does not change if the Boulder region is considered with a linear trend -0.050 ± 0.016 ppm/decade (Figure 1b). However, the 41-year linear trend in the Boulder/FPH record shows instead a clear net increase of 0.47 ppm (linear trend = 0.116 ± 0.003 ppm/decade) from 1980 through 2020, primarily owing to relatively lower mixing ratios during 1980–1990 and relatively higher mixing ratios from 1998 until the sudden drop in 2001. This positive trend cannot be explained even if CLaMS/ERA5 results are interpolated to the locations of the Boulder/FPH observations (green squares). There is still some uncertainty about the degree to which monthly SWV observations over Boulder are representative of the broader NH midlatitude trends (Hegglin et al., 2014; Kunz et al., 2013; Lossow et al., 2017). Because CLaMS/ERA5 output interpolated to Boulder/FPH measurement locations shows almost the same trend as the full CLaMS/ERA5 data set, it is likely that reasons other than sampling representativeness are behind the differences between the Boulder/FPH record and our reanalysis-based results.

To determine whether linear trends derived from the reanalysis-based results are robust, Figure 2 shows their dependence on the choice of the starting year, varying between 1980 and 2010, for both the Tropics and Boulder regions. While there is a very good agreement between the CLaMS/ERA5 and SWOOSH/MLS trends for starting years between the late 1980s and 2010 in the Boulder region, such good agreement is not even evident in the Tropics before the early 2000s. Comparison with the Boulder/FPH shows qualitative agreement only from 2000 to 2004 with positive and statistically significant trends. All reanalysis-based results reproduce the general features of the satellite-based trends although with a large spread (see also Table 1). The reanalyses in general tend to produce trends that are too negative when the starting year is before 1994, indicating that weaker assimilation constraints in the 1980s and 1990s may overestimate the effect of strong volcanic eruptions during this time. As a consequence, positive trends deduced from the Boulder/FPH record cannot be ruled out. As can be deduced from Table 1, trends calculated for the period starting in 2001 show much smaller variability than for the period 1980–2000, when tropical trends ranged between -0.139 (SH/ERA5) and 0.108 (CLaMS/ERAI) ppm/decade

Table 1
Water Vapor Linear Trends (ppm/Decade), Calculated as in Figure 2, and Their 2σ Errors for Two Selected Regions in the Lower Stratosphere (Tropics and Boulder) During Four Periods: 1980–2000 and for Three Periods Starting in 1980/2005/2001 and Ending in 2020 With Exception of the CLaMS Simulations Driven by ERA-Interim (ERAI), MERRA-2 (M2), and JRA-55 (JRA) Which End in 2017 (Tao et al., 2019)

Region	Data	1980–2000	From 1980	From 2001	From 2005
Tropics	CLaMS/ERA5	-0.114 ± 0.058*	-0.065 ± 0.024*	0.188 ± 0.062*	0.090 ± 0.091*
	SH/ERA5	-0.139 ± 0.056*	-0.067 ± 0.023*	0.219 ± 0.060*	0.137 ± 0.088*
	CLaMS/ERAI	0.108 ± 0.052*	0.022 ± 0.026	0.233 ± 0.085*	0.081 ± 0.135
	CLaMS/M2	-0.027 ± 0.058	-0.044 ± 0.027*	0.181 ± 0.084*	0.013 ± 0.130
	CLaMS/JRA	-0.022 ± 0.070	-0.185 ± 0.031*	0.090 ± 0.086*	0.019 ± 0.138
	SWOOSH/MLS			0.130 ± 0.050*	0.089 ± 0.075*
Boulder	CLaMS/ERA5	-0.034 ± 0.038	-0.050 ± 0.016*	0.212 ± 0.037*	0.173 ± 0.050*
	SH/ERA5	-0.107 ± 0.034*	-0.031 ± 0.014*	0.213 ± 0.028*	0.209 ± 0.039*
	CLaMS/ERAI	0.154 ± 0.040*	0.046 ± 0.019*	0.288 ± 0.054*	0.189 ± 0.082*
	CLaMS/M2	-0.073 ± 0.026*	-0.110 ± 0.014*	0.086 ± 0.041*	0.109 ± 0.064*
	CLaMS/JRA	0.027 ± 0.048	-0.159 ± 0.021*	0.065 ± 0.046*	0.095 ± 0.071*
	SWOOSH/MLS			0.199 ± 0.030*	0.180 ± 0.040*
	Boulder/FPH	0.293 ± 0.011*	0.116 ± 0.003*	0.039 ± 0.010*	-0.024 ± 0.012*

Note. Trends which are statistically significant are marked by asterisks. Applying Microwave Limb Sounder averaging kernel on Chemical Lagrangian Model of the Stratosphere/ERA5 output changes the 2005–2020 trend in the Tropics by less than 6%.

and trends in the Boulder region varied between -0.107 (SH/ERA5) and 0.154 (CLaMS/ERAI) or even 0.293 (Boulder/FPH) ppm/decade, with all these extreme values being statistically significant.

Starting from 2001 (or even from 1989 in the Boulder region), good agreement is found between trends based on SWOOSH/MLS and CLaMS/ERA5. Differences with Boulder/FPH are larger. A statistically significant positive trend is found for Boulder/FPH for the 2001–2020 period which is statistically equivalent to the CLaMS/JRA and CLaMS/M2 trends that are weaker than those derived from other simulations (Table 1). Thus, we diagnose a substantial stratospheric moistening of the Tropics, mainly during 2000–2006, with values around 0.15 ppm/decade. A weaker moistening trend of around 0.05 ppm/decade is found after 2006 but is not statistically significant, as the time period over which the trend is calculated is shorter.

Figure 3 shows the global zonal distribution of trends for the full period 1980–2020 (left) and for the years 2001–2020 (right). Linear trends are depicted in the top panels, MLR results in the bottom panels, and the plots show merged stratospheric and tropospheric trends, the former derived from CLaMS/ERA5, the latter from SH/ERA5, using the WMO definition of the tropopause. Particularly striking is a strong positive trend in the upper tropical and Arctic troposphere. Here, water vapor concentrations are expected to rise by approximately 7% per Kelvin as climate warms (Clausius-Clapeyron equation), with larger absolute increases expected where temperatures are either initially low (upper tropical troposphere) or warming is more pronounced (Arctic). Trend values in the stratosphere are much weaker, with significant positive trends identified only for the 2001–2020 period (Figure 3b). Remarkable hemispheric asymmetry is diagnosed, with a stronger positive trend in the Northern Hemisphere and a negative trend over the South Pole. On the other hand, stratospheric trends for the 1980–2020 period are predominantly negative and are noticeably weaker after MLR is applied to remove the moistening contributions of volcanic eruptions and ENSO before 2000 (from Figures 3a–3c). Similarly, the trends after 2000 are also slightly weaker after accounting for these two effects (from Figures 3b–3d; Diallo et al., 2017). In the tropics, the effects of ENSO on SWV dominate those of volcanic eruptions, while the opposite is observed for the extra-tropics.

For validation, we compare linear trends with MLS (Figure 4) for the period 2005–2020 (top panels). We also compare the seasonality of trends for the three selected regions defined by the black rectangles in the left top panel. Tropics and Boulder regions are defined in the same way as before; the Antarctic region is bounded by
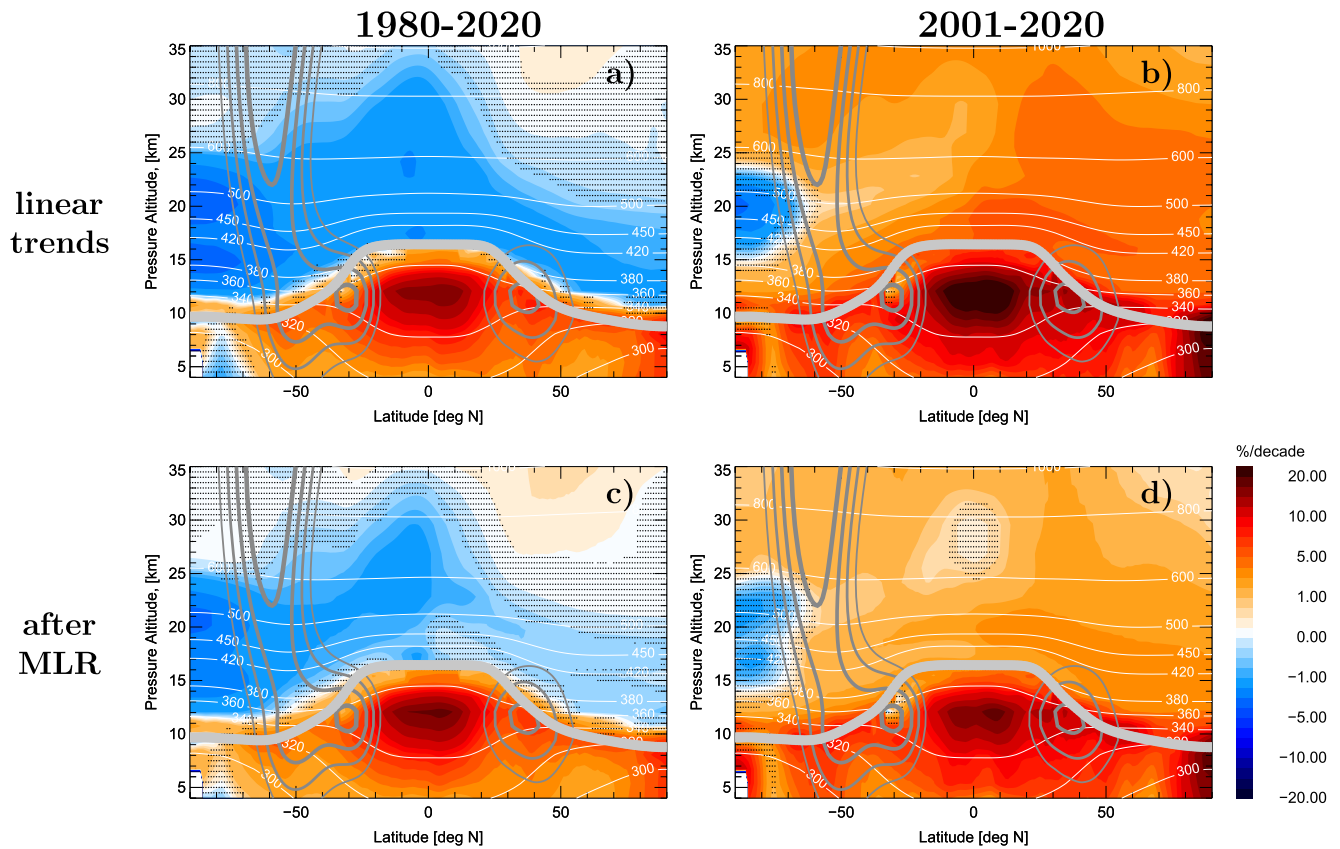
Figure 3. Merged stratospheric and tropospheric trends of zonally averaged water vapor for two periods: 1980–2020 (left) and 2001–2020 (right) in percentage per decade (relative to water vapor mixing ratio averaged over the full period). Below the climatological tropopause (gray thick line), trends are derived from the assimilated specific humidity provided by ERA5, and above they are derived from Chemical Lagrangian Model of the Stratosphere/ERA5 simulation. Top row: linear trends. Bottom row: after removing Quasi-Biennial-Oscillation/El Nino-Southern Oscillation/Aerosol Optical Depth contributions by using multi-linear regression. Trends not statistically different from zero are dot-hatched. Solid gray lines mark climatological westerlies.

latitudes 70°S–90°S and $\theta = 400$–500 K. There are strong similarities and few differences between the MLS and CLaMS/ERA5 based linear trends (Figure 4a vs. Figure 4b). The hemispheric asymmetry is slightly weaker for MLS than for CLaMS/ERA5, with weaker negative trends in the Antarctic stratosphere and weaker positive trends in the NH. Stronger positive trends in the lowermost stratosphere, mainly in the NH, are diagnosed in the CLaMS/ERA5 simulation compared with MLS. On the other hand, the seasonality of the CLaMS/ERA5 trends for three selected regions (middle panels of Figure 4) shows excellent agreement with MLS. Motivated by this agreement, we focus now on a more detailed discussion of these three regions.

The strongest negative trends are found in the Antarctic stratosphere (Figure 4c) from July to September and indicate strengthening dehydration in the winter polar vortex over the last 20 years. However, these trends are not statistically significant at the 95% level. Trends in the tropical lower stratosphere (Figure 4d) show a clear annual cycle. After applying MLR to remove the effects of QBO, ENSO, and volcanic eruptions, this annual cycle is even stronger. This suggests that other drivers are behind the significant positive trends from March to July. While there is very good agreement between CLaMS/ERA5 and MLS seasonal trends, the comparison with Boulder/FPH is worse. In general, the seasonal cycle of trends over Boulder is much weaker than in the tropical and Antarctic stratosphere. There is good agreement between the CLaMS/ERA5 and MLS monthly trends over Boulder, but those based on monthly FPH soundings are weaker and more scattered due to the much smaller number of data points (avg = 21) available to derive them. Trends derived from CLaMS/ERA5 interpolated to the locations of the Boulder/FPH measurements (green open squares in Figure 4e) exhibit much less scatter than is seen in the measured trends (blue filled circles). A systematic shift between the Boulder/FPH and CLaMS/ERA5 or MLS trends is consistent with overlapping statistical 2σ error bars of monthly trends (averaged over all months) shown on the right side of Figure 4e.
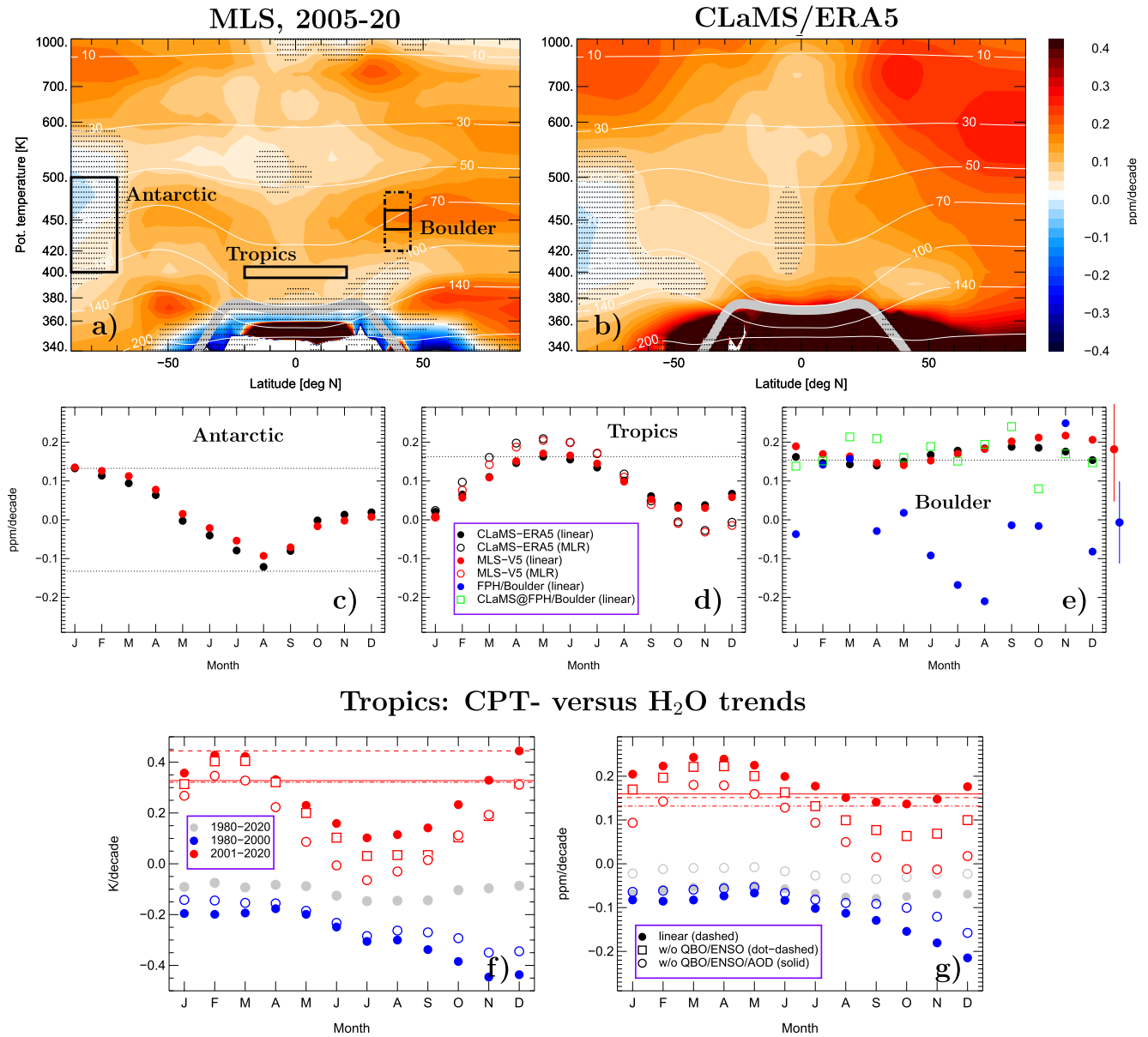
Figure 4. Linear trends as derived from Microwave Limb Sounder (MLS; top left) and Chemical Lagrangian Model of the Stratosphere (CLaMS)/ERA5 for the 2005–2020 period (top right). CLaMS/ERA5 is interpolated to MLS measurement locations with the MLS averaging kernel applied. Results not reaching the level of statistical significance are dot-hatched. The seasonality of the trends for selected regions (black rectangles) is shown in the three middle panels (black—CLaMS/ERA5, red—MLS, and blue—Boulder/FPH). Green open squares in (e) denote the seasonality of CLaMS/ERA5 results interpolated to the Boulder/FPH measurement locations. CLaMS/ERA5 and MLS trend values outside of the dotted black lines are statistically significant. The mean 2σ-errors of the Boulder monthly trends and of the respective MLS trends are shown on the right side of panel (e) as blue and red error bars. With an average of 21 Boulder/FPH data points per monthly trend analysis, the trends have large uncertainties. Seasonality of the cold point temperature (CPT) trend in the tropical lower stratosphere (f) and of the water vapor trend (g) for the 1980–2000 and 2001–2020 periods as well as for the full period 1980–2020. Deseasonalized and boxcar smoothed (width = 5 months) monthly mean CPT anomalies were derived from the ERA5 data as minimum temperatures below $\theta = 450$ K. Stratospheric water vapor and cold point temperature trends for the 2001–2020 period (red) are statistically significant if their values are above the respective horizontal lines describing different multi-linear regression (MLR) configurations (see legend). Trends for periods 1980–2000 and 1980–2020 are not statistically significant. MLR adjustment after removing QBO/ENSO contribution is shown only for the 2001–2020 period.

Finally, we focus on the tropical lower stratosphere as the main entry region of SWV. Figure 4 compares the annual cycle of the SWV trend (g) with that of the CPT (f) for the 2001–2020 period as well as for the 1980–2000 and the full 1980–2020 periods. A pronounced seasonality of both CPT and SWV linear trends stands out for the 2001–2020 period, with a ~0.2 ppm/decade amplitude of the SWV trend corresponding to a ~0.4 K/decade

amplitude of the CPT. The ratio of these two amplitudes is consistent with a rate of 0.5 ppm/K based on the Clausius-Clapeyron equation (Fueglistaler et al., 2014). The peak of the SWV trend annual cycle occurs 1–2 months after that in the CPT trend annual cycle, and is qualitatively consistent with the lag in the water vapor signal associated with diabatic ascent of the tape-recorder signal (Mote et al., 1996). The monthly trends after applying the MLR are weaker, illustrating the importance of the contributions of ENSO and of a few minor extratropical volcanic eruptions (Diallo et al., 2017) to the positive trends in SWV and CPT after 2000. However, even after full MLR adjustment, the seasonality is almost the same as for the linear trend. In contrast, CPT and SWV trends during 1980–2000 were weakly but consistently negative, with much less pronounced, statistically insignificant seasonality, qualitatively explaining the near-zero trends calculated for the full period 1980–2020. We conclude that tropical moistening after 2000 occurred mainly during boreal winter and spring, with statistically significant values exceeding ∼0.15 ppm/decade, and was consistent with warming of the CPT. This effect can only be partially explained by the influences of ENSO and volcanic eruptions after 2000.

4. Conclusions

The importance and applicability of atmospheric reanalyses for climate monitoring are growing. Improved constraints on bias corrections and the ability to assimilate an increasing number of the available observations within a "frozen" data assimilation scheme allow climate variability to be quantitatively evaluated with increasing confidence on timescales of at least a few decades. Here, SWV variability over the last 42 years was reconstructed by using a Lagrangian model framework (CLaMS) driven by the newest ECMWF reanalysis product ERA5. Our analysis shows a robust moistening of the stratospheric overworld that started after the well-documented SWV drop in 2001 (e.g., Randel et al., 2006) and lasted until 2006, with relatively high SWV values persisting over the last decade.

This moistening has occurred mainly in the late boreal winter and spring and is well correlated with warming of the CPT. The latter can only be partially explained by the influences of ENSO and volcanic eruptions, and may be related to ongoing warming of the Earth's surface. There is a clear hemispheric asymmetry in these trends, with the largest positive values in the Northern Hemisphere and evidence of negative trends in the polar Southern Hemisphere. Very good agreement with satellite (MLS, SWOOSH) and fairly good agreement with in situ (Boulder/FPH) observations give us confidence in our results (neither data set is included in the ERA5 assimilation). Considerable moistening of the northern lowermost stratosphere as projected by climate models (Dessler et al., 2013; Keeble et al., 2021) is evident in the reanalysis-based simulations but cannot be unambiguously confirmed by the MLS observations.

SWV trends calculated over the time period 1980–2000 are less robust. Atypical atmospheric conditions associated with major volcanic eruptions and strong ENSO variability during the 1980s and 1990s as well as far fewer observations constraining the reanalysis assimilations may explain both the large spread between the trends derived from different reanalysis-based results and their differences relative to the satellite and in-situ observations. That the CLaMS/ERA5 trends based on zonal (35–45°N) averages and on data interpolated to the Boulder/FPH measurement locations are nearly the same indicates that the discrepancies with the Boulder/FPH-based trends are unlikely to result from representativeness errors in the Boulder data. Although the positive trends of the order 0.10 ppm/decade over the last 41 years as inferred from Boulder/FPH record cannot be excluded (the CLaMS/ERAI trend from 1980 is also weakly positive, although not statistically significant, see Table 1), a full explanation of the differences between the reanalysis-based simulations and Boulder/FPH data is still lacking. The Boulder/FPH record analyzed here is based on only 517 soundings over 41 years, so the observations have much larger sampling uncertainties than zonally averaged MLS or CLaMS data sets with monthly means based on thousands of data points.

We conclude that a robust picture of SWV increases after the sharp drop at the turn of the millennium can be drawn. Weak positive trends associated with the influences of ENSO and volcanic eruptions after 2000 explain less than half of the SWV trend, although there remain some uncertainties in the MLR method that may affect the magnitude of the contributions attributed to these natural factors. Hence, more than half of the moistening after 2000 was likely related to the influences of global warming. The growing quality of the reanalyses on one side and expected future limitations on the availability of high-quality, long-term satellite observations (e.g., the

finite lifetime of MLS with no planned successor) on the other side will strongly encourage the inclusion of future reanalysis products in the monitoring of SWV at climate scales.

Data Availability Statement

MLS data (version 5) used in this paper are retrieved from: https://doi.org/10.5067/Aura/MLS/DATA2508, https://doi.org/10.5067/Aura/MLS/DATA2508. Boulder/FPH data can be downloaded from: https://gml.noaa.gov/aftp/data/ozwv/WaterVapor/Boulder_LEV. CLaMS data used in this paper are described in Tao et al. (2019) and Ploeger et al. (2021). The zonal wind records at 50 and 30 hPa over Singapore used for multi-linear regression (MLR) are provided by: https://www.geo.fu-berlin.de/met/ag/strat/produkte/qbo/qbo.dat. Aerosol extinction coefficient as provided by GLoSSAC v2.0 can be downloaded from the NASA Earthdata Center: https://doi.org/10.5067/GLOSSAC-L3-V2.0, https://doi.org/17/GL0.506OSSAC-L3-V2.0. ERA5 and ERA-Interim model level reanalysis data are available from the ECMWF as deterministic forecasts (atmospheric model): ERA5 via: https://apps.ecmwf.int/data-catalogues/era5/?class=ea, ERA-Interim via: https://apps.ecmwf.int/archive-catalogue/?class=ei). For JRA-55 and MERRA-2 see, JMA (2013) and Global Modeling and Assimilation Office (2015a, 2015b, 2015c), respectively.

References

Banerjee, A., Chiodo, G., Previdi, M., Ponater, M., Conley, A. J., & Polvani, L. M. (2019). Stratospheric water vapor: An important climate feedback. *Climate Dynamics*, *53*(3–4), 1697–1710. https://doi.org/10.1007/s00382-019-04721-4

Brewer, A. W. (1949). Evidence for a world circulation provided by the measurements of helium and water vapour distribution in the stratosphere. *Quarterly Journal of the Royal Meteorological Society*, *75*(326), 351–363. https://doi.org/10.1002/qj.49707532603

Davis, S. M., Hegglin, M. I., Fujiwara, M., Dragani, R., Harada, Y., Kobayashi, C., et al. (2017). Assessment of upper tropospheric and stratospheric water vapor and ozone in reanalyses as part of S-RIP. *Atmospheric Chemistry and Physics*, *17*(20), 12743–12778. https://doi.org/10.5194/acp-17-12743-2017

Davis, S. M., Rosenlof, K. H., Hassler, B., Hurst, D. F., Read, W. G., Vömel, H., et al. (2016). The stratospheric water and ozone satellite homogenized (swoosh) database: A long-term database for climate studies. *Earth System Science Data*, *8*(2), 461–490. https://doi.org/10.5194/essd-8-461-2016

Dee, D. P., Uppala, S. M., Simmons, A. J., Berrisford, P., Poli, P., Kobayashi, S., et al. (2011). The ERA-interim reanalysis: Configuration and performance of the data assimilation system. *Quarterly Journal of the Royal Meteorological Society*, *137*(656), 553–597. https://doi.org/10.1002/qj.828

Dessler, A., Schoeberl, M., Wang, T., Davis, S., & Rosenlof, K. (2013). Stratospheric water vapor feedback. *Proceedings of the National Academy of Sciences*, *110*(45), 18087–18091. https://doi.org/10.1073/pnas.1310344110

Diallo, M., Ploeger, F., Konopka, P., Birner, T., Müller, R., Riese, M., et al. (2017). Significant contributions of volcanic aerosols to decadal changes in the stratospheric circulation. *Geophysical Research Letters*, *44*(2010), 780–810. https://doi.org/10.1002/2017GL074662

Forster, P., & Shine, K. P. (1999). Stratospheric water vapour change as possible contributor to observed stratospheric cooling. *Geophysical Research Letters*, *26*(21), 3309–3312. https://doi.org/10.1029/1999GL010487

Fueglistaler, S., & Haynes, P. H. (2005). Control of interannual and longer-term variability of stratospheric water vapor. *Journal of Geophysical Research*, *110*(D24), D24108. https://doi.org/10.1029/2005JD006019

Fueglistaler, S., Liu, Y., Flannaghan, T., Haynes, P., Dee, D., Read, W., et al. (2013). The relation between atmospheric humidity and temperature trends for stratospheric water. *Journal of Geophysical Research*, *118*(2), 1052–1074. https://doi.org/10.1002/jgrd.5015710.1002/jgrd.50157

Fueglistaler, S., Liu, Y., Flannaghan, T., Ploeger, F., & Haynes, P. (2014). Departure from Clausius-Clapeyron scaling of water entering the stratosphere in response to changes in tropical upwelling. *Journal of Geophysical Research*, *119*(4), 1962–1972. https://doi.org/10.1002/2013JD020772

Fujiwara, M., Wright, J. S., Manney, G. L., Gray, L. J., Anstey, J., Birner, T., et al. (2017). Introduction to the SPARC reanalysis intercomparison project (S-RIP) and overview of the reanalysis systems. *Atmospheric Chemistry and Physics*, *17*(2), 1417–1452. https://doi.org/10.5194/acp-17-1417-2017

Gelaro, R., McCarty, W., Suárez, M. J., Todling, R., Molod, A., Takacs, L., et al. (2017). The modern-era retrospective analysis for research and applications, version 2 (MERRA-2). *Journal of Climate*, *30*(14), 5419–5454. https://doi.org/10.1175/JCLI-D-16-0758.1

Global Modeling & Assimilation Office. (2015a). *MERRA-2 inst3_3d_asm_Np: 3d, 3-hourly, instantaneous, pressure-level, assimilation, assimilated meteorological fields V5.12.4*. Goddard Earth Sciences Data and Information Services Center (GES DISC). https://doi.org/10.5067/QBZ6MG944HW0

Global Modeling, & Assimilation Office. (2015b). *MERRA-2 tavg3_3d_rad_Np: 3d, 3-hourly, time-averaged, pressure-level, assimilation, radiation diagnostics V5.12.4*. Goddard Earth Sciences Data and Information Services Center. (GES DISC). https://doi.org/10.5067/3UGE8WQXZAOK

Global Modeling, & Assimilation Office. (2015c). *MERRA-2 tavg3_3d_tdt_Np: 3d, 3-hourly, time-averaged, pressure-level, assimilation, temperature Tendencies V5.12.4*. Goddard Earth Sciences Data and Information Services Center (GES DISC). https://doi.org/10.5067/9NCR9DDDOPFI

Hegglin, M. I., Plummer, D. A., Shepherd, T. G., Scinocca, J. F., Anderson, J., Froidevaux, L., et al. (2014). Vertical structure of stratospheric water vapour trends derived from merged satellite data. *Nature Geoscience*, *7*(10), 768–776. https://doi.org/10.1038/NGEO2236

Hersbach, H., Bell, B., Berrisford, P., Hirahara, S., Horányi, A., Muñoz-Sabater, J., et al. (2020). The ERA5 global reanalysis. *Quarterly Journal of the Royal Meteorological Society*, *146*(730), 1999–2049. https://doi.org/10.1002/qj.3803

Hurst, D. F., Lambert, A., Read, W. G., Davis, S. M., Rosenlof, K. H., Hall, E. G., et al. (2014). Validation of Aura Microwave Limb Sounder stratospheric water vapor measurements by the NOAA frost point hygrometer. *Journal of Geophysical Research*, *119*(3), 1612–1625. https://doi.org/10.1002/2013JD020757

Hurst, D. F., Oltmans, S. J., Vömel, H., Rosenlof, K. H., Davis, S. M., Ray, E. A., et al. (2011). Stratospheric water vapor trends over Boulder, Colorado: Analysis of the 30 year Boulder record. *Journal of Geophysical Research*, *116*(D2). https://doi.org/10.1029/2010JD015065

Hurst, D. F., Read, W. G., Vömel, H., Selkirk, H. B., Rosenlof, K. H., Davis, S. M., et al. (2016). Recent divergences in stratospheric water vapor measurements by frost point hygrometers and the aura microwave limb sounder. *Atmospheric Measurement Techniques*, *9*(9), 4447–4457. Retrieved from https://amt.copernicus.org/articles/9/4447/2016/

JMA. (2013). *Jra-55: Japanese 55-year reanalysis, daily 3-hourly and 6-hourly data*. Research Data Archive at the National Center for Atmospheric Research, Computational and Information Systems Laboratory. https://doi.org/10.5065/D6HH6H41

Keeble, J., Hassler, B., Banerjee, A., Checa-Garcia, R., Chiodo, G., Davis, S., et al. (2021). Evaluating stratospheric ozone and water vapour changes in CMIP6 models from 1850 to 2100. *Atmospheric Chemistry and Physics*, *21*(6), 5015–5061. https://doi.org/10.5194/acp-21-5015-2021

Kobayashi, S., Ota, Y., Harada, Y., Ebita, A., Morika, M., Onoda, H., et al. (2015). The JRA-55 reanalysis: General specifications and basic characteristics. *Journal of the Meteorological Society of Japan*, *93*(1), 5–48. https://doi.org/10.2151/jmsj.2015-001

Konopka, P., Steinhorst, H.-M., Grooß, J.-U., Günther, G., Müller, R., Elkins, J. W., et al. (2004). Mixing and ozone loss in the 1999-2000 arctic vortex: Simulations with the 3-dimensional chemical Lagrangian model of the stratosphere (CLaMS). *Journal of Geophysical Research*, *109*(D2), D02315. https://doi.org/10.1029/2003JD003792

Kovilakam, M., Thomason, L. W., Ernest, N., Rieger, L., Bourassa, A., & Millán, L. (2020). The global space-based stratospheric aerosol climatology (version 2.0): 1979–2018. *Earth System Science Data*, *12*(4), 2607–2634. https://doi.org/10.5194/essd-12-2607-2020

Kunz, A., Müller, R., Homonnai, V. M., Janosi, I., Hurst, D., Rap, A., et al. (2013). Extending water vapor trend observations over Boulder into the tropopause region: Trend uncertainties and resulting radiative forcing. *Journal of Geophysical Research*, *118*(1911), 269284–269311. https://doi.org/10.1002/jgrd.50831

Li, F., & Newman, P. (2020). Stratospheric water vapor feedback and its climate impacts in the coupled atmosphere–ocean Goddard Earth Observing System Chemistry-Climate Model. *Climate Dynamics*, *55*(5–6), 1585–1595. https://doi.org/10.1007/s00382-020-05348-6

Livesey, N. J., Read, W. G., Froidevaux, L., Lambert, A., Santee, M. L., Schwartz, M. J., et al. (2021). Investigation and amelioration of long-term instrumental drifts in water vapor and nitrous oxide measurements from the Aura Microwave Limb Sounder (MLS) and their implications for studies of variability and trends. *Atmospheric Chemistry and Physics*, *21*(20), 15409–15430. https://doi.org/10.5194/acp-21-15409-2021

Livesey, N. J., Read, W. G., Wagner, P. A., Froidevaux, L., Santee, M. L., Schwartz, M. J., et al. (2020). *Version 5.0x level 2 and 3 data quality and description document (Tech. Rep. No. JPL D-105336 Rev. A). Jet Propulsion Laboratory*. California Institute of Technology Pasadena. Retrieved from http://mls.jpl.nasa.gov

Lossow, S., Khosrawi, F., Nedoluha, G. E., Azam, F., Bramstedt, K., Burrows, J. P., et al. (2017). The SPARC water vapour assessment ii: Comparison of annual, semi-annual and quasi-biennial variations in stratospheric and lower mesospheric water vapour observed from satellites. *Atmospheric Measurement Techniques*, *10*(3), 1111–1137. https://doi.org/10.5194/amt-10-1111-2017

McKenna, D. S., Konopka, P., Grooß, J.-U., Günther, G., Müller, R., Spang, R., et al. (2002). A new Chemical Lagrangian Model of the Stratosphere (CLaMS) 1. Formulation of advection and mixing. *Journal of Geophysical Research*, *107*(D16). https://doi.org/10.1029/2000JD000114

Mote, P. W., Rosenlof, K. H., McIntyre, M. E., Carr, E. S., Gille, J. G., Holton, J. R., et al. (1996). An atmospheric tape recorder: The imprint of tropical tropopause temperatures on stratospheric water vapor. *Journal of Geophysical Research*, *101*(D2), 3989–4006. https://doi.org/10.1029/95jd03422

Müller, R., Kunz, A., Hurst, D. F., Rolf, C., Krämer, M., & Riese, M. (2016). The need for accurate long-term measurements of water vapor in the upper troposphere and lower stratosphere with global coverage. *Earth's Future*, *4*(2), 25–32. https://doi.org/10.1002/2015EF000321

Oltmans, S. J., Vömel, H., Hofmann, D. J., Rosenlof, K. H., & Kley, D. (2000). The increase in stratospheric water vapor from balloonborne, frostpoint hygrometer measurements at Washington, D.C., and Boulder, Colorado. *Geophysical Research Letters*, *27*(21), 3453–3456. https://doi.org/10.1029/2000GL012133

Ploeger, F., Diallo, M., Charlesworth, E., Konopka, P., Legras, B., Laube, J. C., et al. (2021). The stratospheric Brewer–Dobson circulation inferred from age of air in the ERA5 reanalysis. *Atmospheric Chemistry and Physics*, *21*(11), 8393–8412. https://doi.org/10.5194/acp-21-8393-2021

Pommrich, R., Müller, R., Grooß, J.-U., Konopka, P., Ploeger, F., Vogel, B., et al. (2014). Tropical troposphere to stratosphere transport of carbon monoxide and long-lived trace species in the Chemical Lagrangian Model of the Stratosphere (CLaMS). *Geoscientific Model Development*, *7*(6), 2895–2916. https://doi.org/10.5194/gmd-7-2895-2014

Randel, W. J., & Park, M. (2019). Diagnosing observed stratospheric water vapor relationships to the cold point tropical tropopause. *Journal of Geophysical Research*, *124*(13), 7018–7033. https://doi.org/10.1029/2019JD030648

Randel, W. J., Wu, F., Vömel, H., Nedoluha, G. E., & Forster, P. (2006). Decreases in stratospheric water vapor after 2001: Links to changes in the tropical tropopause and the Brewer-Dobson circulation. *Journal of Geophysical Research*, *111*(D12). https://doi.org/10.1029/2005JD006744

Rosenlof, K. H., Oltmans, S. J., Kley, D., Russell, J. M., III, Chiou, E.-W., Chu, W. P., et al. (2001). Stratospheric water vapor increases over the past half-century. *Geophysical Research Letters*, *28*(7), 1195–1198. https://doi.org/10.1029/2000GL012502

Smith, J. W., Haynes, P. H., Maycock, A. C., Butchart, N., & Bushell, A. C. (2021). Sensitivity of stratospheric water vapour to variability in tropical tropopause temperatures and large-scale transport. *Atmospheric Chemistry and Physics*, *21*(4), 2469–2489. https://doi.org/10.5194/acp-21-2469-2021

Solomon, S., Rosenlof, K., Portmann, R., Daniel, J., Davis, S., Sanford, T., & Plattner, G.-K. (2010). Contributions of stratospheric water vapor to decadal changes in the rate of global warming. *Science*, *327*(5970), 1219–1223. https://doi.org/10.1126/science.1182488

Stenke, A., Dameris, M., Grewe, V., & Garny, H. (2009). Implications of Lagrangian transport for simulations with a coupled chemistry-climate model. *Atmospheric Chemistry and Physics*, *9*(15), 5489–5504. Retrieved from http://www.atmos-chem-phys.net/9/5489/2009/

Tao, M., Konopka, P., Ploeger, F., Yan, X., Wright, J. S., Diallo, M., et al. (2019). Multitimescale variations in modeled stratospheric water vapor derived from three modern reanalysis products. *Atmospheric Chemistry and Physics*, *19*(9), 6509–6534. https://doi.org/10.5194/acp-19-6509-2019

Tegtmeier, S., Anstey, J., Davis, S., Dragani, R., Harada, Y., Ivanciu, I., et al. (2020). Temperature and tropopause characteristics from reanalyses data in the tropical tropopause layer. *Atmospheric Chemistry and Physics*, *20*(2), 753–770. https://doi.org/10.5194/acp-20-753-2020

Thomason, L. W. (2020). *Global space-based stratospheric aerosol climatology version 2.0NASA Langley atmospheric science data center DAAC*. Retrieved from https://asdc.larc.nasa.gov/project/GloSSAC/GloSSAC_2.0

Wang, T., Zhang, Q., Hannachi, A., Hirooka, T., & Hegglin, M. I. (2020). Tropical water vapour in the lower stratosphere and its relationship to tropical/extratropical dynamical processes in ERA5. *Quarterly Journal of the Royal Meteorological Society*, *146*(730), 2432–2449. https://doi.org/10.1002/qj.3801

Wolter, K., & Timlin, M. S. (2011). El nino/southern oscillation behaviour since 1871 as diagnosed in an extended multivariate enso index (mei.ext). *International Journal of Climatology*, *31*, 1074–1087. https://doi.org/10.1002/joc.2336

Wright, J., Fujiwara, M., Long, C., Anstey, J., Chabrillat, S., Compo, G. P., et al. (2022). *Chapter 2: Description of the reanalysis systems, SPARC Report No. 10, WCRP Report 6/2021 (Tech. Rep.)*. SPARC Office. https://doi.org/10.17874/800DEE57D13